PCCP

Accepted Manuscript

This is an *Accepted Manuscript*, which has been through the Royal Society of Chemistry peer review process and has been accepted for publication.

Accepted Manuscripts are published online shortly after acceptance, before technical editing, formatting and proof reading. Using this free service, authors can make their results available to the community, in citable form, before we publish the edited article. We will replace this *Accepted Manuscript* with the edited and formatted *Advance Article* as soon as it is available.

You can find more information about *Accepted Manuscripts* in the Information for Authors.

Please note that technical editing may introduce minor changes to the text and/or graphics, which may alter content. The journal's standard Terms & Conditions and the Ethical guidelines still apply. In no event shall the Royal Society of Chemistry be held responsible for any errors or omissions in this *Accepted Manuscript* or any consequences arising from the use of any information it contains.

ROYAL SOCIETY OF CHEMISTRY

www.rsc.org/pccp

Supercell approach to doping effect on thermoelectric properties of SnSe

Yasumitsu Suzuki[1, 2, †], Hisao Nakamura*[1, 2]

[1] National Institute of Advanced Industrial Science and Technology (AIST), 1-1-1 Umezono, Tsukuba, Ibaraki 305-8568, Japan

[2] Thermal Management Materials and Technology Research Association (TherMAT)

[†] Present address: Department of Physics, Tokyo University of Science, 1-3 Kagurazaka, Shinjuku-ku, Tokyo 162-8601, Japan

*H.N. e-mail: hs-nakamura @ aist.go.jp

Physical Chemistry Chemical Physics Accepted Manuscript

ABSTRACT

We study the thermoelectric properties of tin selenide (SnSe) by using first-principles calculations coupled with the Boltzmann transport theory. A recent experimental study showed that SnSe gives an unprecedented thermoelectric figure of merit ZT of 2.6 ± 0.3 in the high-temperature (> 750 K) phase, while ZT in the low-temperature phase (< 750 K) is much smaller than that of high-temperature phase. Here we explore the possibility to increase ZT in the low-temperature regime by carrier doping. For this purpose, we adopt a supercell approach to model the doped systems. We first examine the validity of the conventional rigid-band approximation (RBA), and then calculate thermoelectric properties of Ag or Bi doped SnSe as p- or n-type doped materials using our supercell method. We found that both types of doping improve ZT and/or the power factor of the low-temperature phase SnSe, but only after the adjustment of the proper doping level is achieved.

Physical Chemistry Chemical Physics Accepted Manuscript

I. INTRODUCTION

Energy harvesting by using waste heat is one of the most important issues and design of efficient thermoelectric materials optimized in low-middle temperature regime is highly demanded.[1-3] The efficiency of thermoelectric materials is quantified by the dimensionless figure of merit,

$$ZT = \frac{S^2\sigma}{\kappa_e+\kappa_l}T, \tag{1}$$

where S is the Seebeck coefficient (or the thermopower), σ is the electrical conductivity, κ_e is the electronic contribution to the thermal conductivity while κ_l is the lattice contribution to the thermal conductivity, and T is the absolute temperature. Although it is a challenging task to achieve high ZT value since S, σ and κ_e are strongly interconnected, new strategies and materials have been proposed and devised over the last decades.[1-3]

One important issue has been to find or develop the materials that have high power factor (PF) $S^2\sigma$. While the ZT characterize the energy conversion efficiency of the material, the PF quantifies the actual electrical power produced by a given temperature difference. It is also a key quantity to be enhanced, especially when we consider recovering plenty of waste heat at low temperatures where not only the efficiency but the actual electrical power produced is also important. The improvement of the PF is often realized by band engineering with suitable doping to the materials.[4] Another important strategy to improve the thermoelectric efficiency is to reduce the lattice thermal conductivity κ_l, which can be modified in a relatively independent way without affecting other quantities S, σ and κ_e. The basic idea to reduce the κ_l has been employing heavy-metal-based materials, such as Bi_2Te_3 and PbTe, which indeed have been the best thermoelectric materials working at low and middle temperatures until now and give high ZT value close to 1. Further strategy is to increase phonon scattering, by engineering nanostructures,[5] or making the phonon-glass-electron-crystal (PGEC) materials, whose complex unit cells realize glasslike thermal transport and crystal-like electron transport.[6-10] However, these materials usually contains the elements which are toxic and/or scarce and very expensive. Therefore there is a significant demand to prepare alternative materials which are toxic elements free and scarce elements free to actualize large-scale applications and commercial deployment of the thermoelectric devices. One prospective direction is developing organic semiconducors[11-14] and molecular junctions[15-18] as

Physical Chemistry Chemical Physics Accepted Manuscript

thermoelectric materials, although *ZT* of these organic materials are still small[19]. There are many expectations that organic thermoelectric materials will be further developed.

On the other hand, recently, relatively light-element-based inorganic materials which has rather simple crystal structures have been reported to give extraordinary high ZT value.[20] The examples are cupper selenide ($Cu_{2-x}Se$)[21, 22] and tin selenide (SnSe),[23-25] which found to have very interesting features which reduce the lattice thermal conductivity κ_l significantly. Cupper selenide ($Cu_{2-x}Se$) has the feature of the high degree disorder of the Cu^{I} ions which can move through the rigid face-centered cubic lattice of Se at high temperatures. This results in a new concept, so-called phonon-liquid-electron-crystal (PLEC), which greatly reduces the κ_l. However this diffusion of ions also causes severe degradation of the material,[26] which pose a problem to be solved for practical applications.

Tin selenide (SnSe), on the other hand, also showed to give remarkably high *ZT* in a relatively stable manner.[23-25] Single crystal of SnSe has a layered orthorhombic crystal structure which undergoes a phase transition at ~750-800K between its high temperature higher symmetry (space group *Cmcm*) phase and its low temperature lower symmetry (space group *Pnma*) phase,[27, 28] and Zhao et al. showed that the high-temperature *Cmcm* phase gave a *ZT* approximately 2.6 at 923 K along a particular crystallograpfic direction.[23] This *ZT* comes from ultralow lattice thermal conductivity κ_l, which stems from the strong anharmonicity of chemical bonds.

While the high-temperature *Cmcm* phase of single crystal SnSe was found to show very high *ZT*, it was also reported that its low-temperature *Pnma* phase gives relatively moderate or small *ZT* around 0.12 (at 300K) to 1.25 (at 750K). But for practical waste-heat recovery in automotive exhausts, industrial plants and home heating, it is desirable to have thermoelectric materials which operate efficiently at this low or middle temperature range (300K - 750K). Therefore it is highly demanded to improve *ZT* value of the low-temperature phase of SnSe. Since the *ZT* value reported by Zhao et al.[23] was for the undoped single crystal SnSe without any optimization of the carrier concentration, there is much hope to enhance *ZT* by doping. Very recently experimental study which attempts to improve thermoelectric efficiency of polycrystalline SnSe by doping have been conducted.[24]

Physical Chemistry Chemical Physics Accepted Manuscript

Physical Chemistry Chemical Physics Accepted Manuscript

In this study we perform theoretical investigations based on the first-principles band structure calculations and the Boltzmann transport theory to elucidate how dopants modify the band structure and thermoelectric property of the low-temperature phase of single crystal SnSe. In recent years, a number of study have been performed using the first principle band structure calculations coupled with the Boltzmann transport theory to investigate thermoelectric properties of various kinds of bulk materials as well as design of dopant,[29-47] The rigid band approximation (RBA), i.e., fixed band structure and shifting chemical potential, is often adopted due to computational convenience. And in fact, very recently Boltzmann transport calculation with RBA have been applied to study the thermoelectric properties of SnSe and the doping effect on it, and many useful information have been elucidated.[48-51] However validity of RBA is not necessarily clear for a practical material design. Careful analysis by detailed first principles calculations of the system including explicit dopant elements is desirable before performing large scale material simulation by RBA.

To perform systematic analysis, we construct the supercells of SnSe and carry out the thermoelectric property calculations for the large unitcells which explicitly contain the dopant atoms. For the calculation of electrical conductivity σ, Seebeck coefficient S and electronic contribution to the thermal conductivity κ_e using Boltzmann transport theory, we employ the method of the Fourier interpolation of the bands developed by Madsen and Singh,[30] but in order to calculate the doped supercell we slightly modify the method such that it does not use the space group symmetry of the unitcell. We show our Boltzmann transport calculation successfully reproduce the experimental data of the single crystal SnSe reported by Zhao et al.[23] We also check numerical accuracy of our band interpolation scheme where the space group symmetry is not assumed. Then we calculate the Ag or Bi doped SnSe (1×3×3) supercell and (1×4×4) supercell as p- or n-type doped materials, and show the RBA fails in this case and how these doping affects the thermoelectric property of SnSe, predicting the *ZT* and/or PF will be improved if the proper doping level is achieved.

This paper is organized as follows. In section II, we explain our computational approach to calculate thermoelectric property of the doped-SnSe systems using the supercell method. In section III, first we present the results of the thermoelectric property calculation for the undoped single crystal SnSe in its low temperature phase. Then we show the results of the doping dependent thermoelectric properties obtained using the RBA. Finally, we present the results of our supercell calculations, showing its effectiveness to study how the doping affects thermoelectric properties. In section IV we summarize the results and remark on the future directions.

Physical Chemistry Chemical Physics Accepted Manuscript

II. COMPUTATIONAL APPROACH

In this section we summarize our computational approach to calculate thermoelectric property of SnSe supercell. Within the linear response theory, the electric conductivity, thermal conductivity, and Seebeck coefficient can be derived by the Onsager coefficients. Based on the Boltzmann transport theory, the set of Onsager coefficients is calculated by using the group velocity $\boldsymbol{v}$ and the relaxation time τ. To calculate group velocities, we construct the analytic representation of band energies using the algorithm developed by Madsen and Singh and implemented in BOLTZTRAP code.[30] It is based on the smoothed Fourier interpolation of the band energies obtained by the first-principles band structure calculation. In this study we aim to calculate thermoelectric properties of the Bi or Ag doped-SnSe supercells, i.e., the size of the unit cell is large and has only low-symmetry. Hence, we adopt SIESTA[52] program package for the band calculation and pass the data to our in-house interface code of BOLTZTRAP to interpolate the band structure. All of the band structure calculations are performed by DFT with PBE functional[53] and a double zeta plus polarized function (DZP) is used as basis set. In our in-house program, the interpolation algorithm is slightly modified from the original one implemented in BOLTZTRAP; we expand the band-energies as $\sum_{\mathbf{R}_\mathbf{m}} C_i(\mathbf{R}_m) S_{\mathbf{R}_m}(\mathbf{k})$, where $\mathbf{R}_m$ is a direct lattice vector and $S_{\mathbf{R}_m}(\mathbf{k}) = \exp[i\mathbf{R}_m \cdot \mathbf{k}]$, which does not include the symmetry operators. Thus it can be applied to any low-symmetry unit cells. To check numerical error caused by increasing system (band data) size, we compared the result of the primitive cell and that of the supercell (without using symmetry), which consists of more than nine primitive cells, for the same SnSe *Pnma* crystal, then we confirmed sufficient numerical accuracy. We note that our interpolation scheme become difficult when the band structure consist of many band crossing. Then an alternative approach will be required e.g., the method using the momentum matrix elements $\langle \psi_{i,\boldsymbol{k}} | \hat{p} | \psi_{i,\boldsymbol{k}} \rangle$.[29,33,54] The other key parameter is the relaxation time τ. The electrons are scattered by several mechanisms like acoustic phonons, optical phonons, impurities,...etc, and the total relaxation time τ obeys Matthiessens's rule

$$\frac{1}{\tau} = \frac{1}{\tau_{\mathrm{ac}}} + \frac{1}{\tau_{\mathrm{op}}} + \frac{1}{\tau_{\mathrm{imp}}} + \cdots \qquad (2)$$

While there are several methods to evaluate the relaxation time,[12,55] it is still challenging task to derive each factor of relaxation time via first principles calculation.

Physical Chemistry Chemical Physics Accepted Manuscript

In this study we adopt the following analytical model[56-60]

$$\tau(T,\epsilon) = \tau_{\mathrm{ref}}\left(\frac{T_{\mathrm{ref}}}{T}\right)^{r-1/2}\left(\frac{\epsilon-\mu}{k_B T}\right)^{r-1/2}. \qquad (3)$$

The model is derived by parabolic band[24] and is assuming that dominant relaxation mechanism triggered by scattering with acoustic phonons (r = 0), which is observed experimentally by Snyder et al.[24] We set τ_{ref} = 40 fs, T_{ref} = 300 K. μ is the chemical potential at T_{ref} in the present study. We found the present simple analytical model improved the agreement between calculated and experimental results largely comparing with those of constant τ approximation. Hence, we adopt this model for the entire calculations.

Physical Chemistry Chemical Physics Accepted Manuscript

Physical Chemistry Chemical Physics Accepted Manuscript

III. RESULTS AND DISCUSSION

A. Thermoelectric properties of the undoped SnSe

First we show the results of the thermoelectric property calculations for the undoped single crystal SnSe in its low-temperature *Pnma* phase.

The crystal structure is presented in Figure 1. Along the b-c plane, it has two-atom-thick SnSe slabs, which are corrugated and creates a zig-zag accordion-like projection along the b axis.[61-62] The slabs are connected with weak Sn-Se bonding along the a direction. We performed geometry optimization by relaxing both of cell size and atomic positions, and the obtained lattice constants are a=11.82 Ǻ, b=4.26 Ǻ and c=4.59 Ǻ, respectively. They are in good agreement with the experimental data (a=11.50 Ǻ, b=4.15 Ǻ and c=4.45 Ǻ).[61,62] In Figure 2 we present the calculated band structure. The band structure of SnSe is quite similar with that of SnS, which is reported by Singh et al.[31] There is a heavy-mass band below the Fermi level connecting U and Z points, which is expected to give a high Seebeck coefficient. It is also anticipated that the heavy-mass band oriented along the x-direction along U-Z direction produces the low conductivity in the x-direction, which is indeed observed in the experiment.[23] Since p-doped SnS was reported as a good thermoelectric material,[63] it is expected that thermoelectric properties of SnSe can be improved by the same doping technique. The calculated band gap is 0.44 eV, which is smaller than the experimental value 0.86 eV reported by Zhao et al.,[23] due to use of PBE functional. Since the correct bandgap is critical for the evaluation of thermoelectric properties, we apply a scissor operator to rigidly shift the conduction bands such that the value of the bandgap coincides with the experimental value 0.86 eV.

In Figure 3 we show the calculated results of σ, S, the power factor (PF) $S^2\sigma$, the electric thermal conductivity κ_e and the thermoelectric figure of merit ZT of the *Pnma* undoped SnSe crystal as functions of temperature. Note that we evaluated these thermoelectric properties for each (a, b, and c) axial direction. We set the carrier (hole) concentration of the system as 6×10^{17} cm^{-3}, which is the value obtained from the experimental Hall measurements at 300 K.[23] The carrier concentration is determined by

$$n = \int D(\epsilon)\frac{1}{\exp[(\epsilon-\mu)/k_BT]+1}d\epsilon, \qquad (4)$$

where n is the number of electrons in the unit cell, $D(\epsilon)$ is DOS, and k_B is Boltzmann constant. Here chemical potential μ is a parameter to adjust n. In order to calculate ZT, the lattice thermal conductivity κ_l is required. In this study, we estimated κ_l by taking the difference between the experimental value of the total thermal conductivity, $\kappa_{\mathrm{tot}}^{\mathrm{Exp}}$,[23] and the calculated κ_e, i.e., $\kappa_l(T) = \kappa_{\mathrm{tot}}^{\mathrm{Exp}}(T) - \kappa_e(T)$.

All of our calculated properties in Fig. 3 are in reasonable agreement with the experimental values in Ref. 23, which are also plotted in Fig. 3 with open circles (a axis: red circle, b axis: green circle, c axis: blue circle). We emphasize that our results reproduce the anisotropy of σ, PF and ZT (higher values along b axis and c axis, and reduced value along a axis), and hence, we conclude that our computational approach and introduced approximation are valid sufficiently for the present study. To figure out contribution of the lattice thermal conductivity, we also calculated $Z_{\mathrm{e}}T = \frac{S^2\sigma}{\kappa_e}T$, which is figure of merit omitting κ_l (the bottom of the left panel in Fig. 3). We find significant difference between Z_eT and ZT. This difference comes from the fact that κ_e is very small compared to κ_l in this *undoped*-SnSe case. Furthermore, we observe that Wiedemann-Franz (WF) law fails at higher temperatures in this system. WF law predicts the approximated value of the electronic contribution to thermal conductivity κ_e^{WF} is given by

$$\kappa_e^{\mathrm{WF}} = L\sigma T \tag{5}$$

where the Lorenz number $L = \frac{\pi^2}{3}\left(\frac{k_B}{e}\right)^2 = 2.44 \times 10^{-8}\,\mathrm{W\Omega K^{-2}}$. Note that Eq. (5) is the result of electron gas and usually only holds for simple metals. However, deviation from WF law is useful index to design high ZT materials by means of band-engineering. Hence we compare κ_e and κ_e^{WF} for the present SnSe system. We plot it in the right middle panel of Fig. 3 for all of the three axial directions (a axis: gray solid, b axis: orange dashed, c axis: black dotted) and find it deviates from the correct value especially at higher temperatures, showing the violation of the WF law.

Physical Chemistry Chemical Physics Accepted Manuscript

B. Analysis of doping effect by rigid-band approximation

From now on, we analyze the doping effect on the thermoelectric properties of the low-temperature phase SnSe. First we apply the rigid-band approximation (RBA).

In Figure 4, σ, S, PF, κ_e, and ZT at 300K and 450K of the doped SnSe calculated by the RBA are plotted as a function of carrier concentration. Positive value of the carrier concentration corresponds to the holes (p-type doping), and the negative corresponds to the electrons (n-type doping). In the present study, we omitted change of κ_l by doping, i.e., κ_l was fixed at the value used for the undoped SnSe. The doping often reduces κ_l: thus the present κ_l will overestimate the exact value of doped system. In addition, we employ the same relaxation time model (Eq. (3)) and consider only scattering by acoustic phonons for all doping levels. This is somewhat crude approximation. However, our main focus is to analyze the tendency of thermoelectric properties upon carrier doping as well as effect of local chemical structure by different doped chemical specie (i.e., validity of RBA). More rigorous derivation of κ_l and τ is out of the scope in the present study. Therefore we use the same relaxation time model throughout this work.

In (e) and (f) of Fig. 4, it is seen anisotropic enhancements of PF occur by the dopings. N-type doping gives the largest PF along the a-axis direction while p-type doping gives the largest PF along the b-axis. This anisotropic enhancement of the PF is caused by different response to the electrical conductivity σ by carrier doping, which are shown in (a) and (b) of Fig. 4. The values of κ_e^{WF} (Eq. (5)) are also plotted in (g) and (h). We find κ_e^{WF} again deviates from the correct κ_e, but it reproduces the overall tendency. Enhancement of ZT value is also achieved by doping, particularly, when the carrier concentration is around 5×10^{19} cm^{-3} - 5×10^{20} cm^{-3} for both p and n type doping. Note that ZT reduces significantly by further increasing carrier concentration since κ_e become further large (see (g) and (h)) and Seebeck coefficients S become very small (see (c) and (d)). Thus control of the optimized doping level is crucial to improve ZT and/or the PF, according to the above analysis based on the RBA.

Physical Chemistry Chemical Physics Accepted Manuscript

Physical Chemistry Chemical Physics Accepted Manuscript

C. Doping of Bi and Ag via supercell model calculation

As described in the previous subsection, RBA is a simple and conventional approach for rough design of material by doping. However, validity of RBA is not clear for SnSe. Seebeck coefficient S is sensitive to the transport distribution function (TDF)[29,30], which is defined as

$$\sigma_{\alpha\beta}(\varepsilon) = \frac{e^2}{N}\sum_{i,\mathbf{k}} \tau(i,\mathbf{k}) \cdot v_\alpha(i,\mathbf{k}) \cdot v_\beta(i,\mathbf{k}) \cdot \delta(\varepsilon - \varepsilon_{i,\mathbf{k}}) \tag{6}$$

where $v_\alpha(i,\mathbf{k})(\alpha = x, y, z)$ is the α-th component of the group velocity; $v_\alpha(i,\mathbf{k}) = \frac{1}{\hbar}\frac{\partial \varepsilon_{i,\mathbf{k}}}{\partial k_\alpha}$, i.e., Seebeck coefficient is strongly dependent on the band structures near the chemical potential. Since dopant sometimes makes new chemical/ionic bonding and changes local electronic structures, careful assessment of error of RBA is quite important to evaluate the thermoelectric properties correctly. To elucidate the validity of RBA and suggest more practical material design by dopant, we introduce the supercell model to represent the doped SnSe. Here we examine Bi and Ag as n and p-type dopant respectively. We construct the supercell which consists of the (1×3×3) and/or (1×4×4) primitive unit cell of SnSe, and replace one Sn atom with X (=Bi or Ag). The composition of the former case is represented as $X_{0.028}Sn_{0.972}Se$ and the latter is $X_{0.016}Sn_{0.984}Se$. These compositions correspond to the values of electron/hole concentration 4.79×10^{20} cm^{-3} and 2.69×10^{20} cm^{-3} respectively. According to the calculated results by the RBA, these values should improve performance of PF and ZT, though they are not the most optimized doping concentration.

The calculated band structures of $Bi_{0.028}Sn_{0.972}Se$ (green solid line) and $Ag_{0.028}Sn_{0.972}Se$ (blue solid line) are shown in Fig. 5. In the figure the whole bands are rigidly shifted along y-axis so that the chemical potential at 300K is located at zero for each system. The band of the undoped SnSe (1×3×3) supercell is also plotted (red dashed line) for a comparison. Note that in the present study the same scissor operator is applied to all systems, i.e., the bands above the band gap are always shifted the same value that is employed for the undoped SnSe. It also should be noted that Fig. 5 shows the conduction bands consists of both parabolic bands and non-parabolic bands, but we still rely on the relaxation time based on a parabolic band model Eq. (3).[48, 56-60] Comparing green/bule solid line and red dashed line in Fig. 5, it is found considerable changes of band structures take place in both doped SnSe from the undoped one.

Especially the changes are significant around the CBM in the $Bi_{0.028}Sn_{0.972}Se$ case and around the VBM in the $Ag_{0.028}Sn_{0.972}Se$ case, respectively. Since the band structures close to CBM/VBM are critical to thermoelectric property as discussed above, we conclude that the application of the RBA is not suitable for SnSe.

Calculated thermoelectric properties of $Bi_{0.028}Sn_{0.972}Se$ and $Ag_{0.028}Sn_{0.972}Se$ are presented as a function of temperature in Fig. 6. Enhancement of PF along a axis is found for $Bi_{0.028}Sn_{0.972}Se$ while PF along b axis is increased in $Ag_{0.028}Sn_{0.972}Se$ over the entire temperature region. However the degree of the enhancement is smaller than calculated by RBA. Temperature dependence of κ_e is similar with that of PF. There are deviations from WF law in both systems, in particular, WF law overestimates κ_e of Ag doped system. As overall tendency, *ZT* of Ag doped system is larger than that of Bi doped system; however, they are suppressed comparing with those obtained by the RBA in both cases.

As described by the RBA calculations, *ZT* is potentially very sensitive to the amount of carrier concentration. PF and *ZT* obtained by the explicit supercell calculations are slightly smaller than those of the RBA results. In addition, we found the tendency that the optimized carrier concentration for *ZT* predicted by the RBA is overestimated. Hence we examine the lower-doped SnSe systems, i.e., $Bi_{0.016}Sn_{0.984}Se$ and $Ag_{0.016}Sn_{0.984}Se$. The resultant σ, S, PF, κ_e, κ_e^{WF} and *ZT* values are given in Figure 7. As shown in Figs. 6 and 7, reduction of doping rate does not affect the PF so much in the Bi-doping case and enhance the PF along b axis in the Ag-doping case. On the other hand, the κ_e are largely reduced in both cases. WF law reproduces the tendency of κ_e, but there are non-negligible deviations especially along b axis in the Ag-doping case. In total, higher *ZT* is achieved by reducing doping level from $X_{0.028}Sn_{0.972}Se$ to $X_{0.016}Sn_{0.972}Se$ as expected. Particularly, reducing Ag dopant rapidly improves *ZT* along a axis and b axis with increasing temperature (~ 750 K). We anticipate that *ZT* will be further enhanced by controlling the doping level.

Physical Chemistry Chemical Physics Accepted Manuscript

IV. CONCLUSIONS AND OULOOK

We applied first principles calculation coupled with Boltzmann transport theory to study thermoelectric properties of low temperature phase SnSe. Design of high *ZT* by doping was examined by both the rigid-band approximation and the supercell approach, where Bi and Ag dopants were adopted as n and p type doping respectively. To apply Boltzmann method to the low-symmetry crystal (and/or large super cell), we developed the numerical method which does not use the space-group symmetry of the unit cell, and showed that our approach successfully reproduces the experimental thermoelectric property data reported by Zhao et al.[23] We found the rigid band approximation is not valid to evaluate *ZT* etc. for the doped SnSe systems. The results from the supercell approach indicate the possibility of improving *ZT* and/or PF by doping, but precise control of doping level is required. It is indicated that exceed of carrier concentration reduces *ZT* rapidly. We also clarified how Wiedemann-Franz law is violated in this SnSe system. We found Ag-doped SnSe gives higher *ZT* than that of Bi-doped SnSe.

It should be noted that more rigorous evaluation of the relaxation time τ than Eq. (3) is desirable for quantitative evaluation of *ZT* etc., which might be possible e.g., by incorporation of first principles nonequilibrium Green's function theory into Boltzmann method. In addition, relation of doping level and lattice thermal conductivity κ_l as well as phonon-phonon scattering[64, 65] is the scope of the future study for thermoelectric material design by first principles approach.

Physical Chemistry Chemical Physics Accepted Manuscript

ACKNOELEDGEMENTS

We acknowledge fruitful discussion with Dr. Yoshihiro Asai. This work was supported by Thermal Management Materials and Technology Research Association (TherMAT), Future Pioneering Projects of the Ministry of Economy, Trade and Industry, Japan. H. N. also thanks to Cooperative Research Program of “Network Joint Research Center of Materials and Devices”.

Physical Chemistry Chemical Physics Accepted Manuscript

REFERENCES

(1) G. J. Snyder and E. S. Toberer, Nature Mater. 7, 105 (2008).

(2) M. G. Kanatzidis, Chem. Mater. 22, 648 (2010).

(3) J. P. Heremans and M. S. Dresselhaus and L. E. Bell and D. T. Morelli, Nature Nanotechnol. 8, 471 (2013).

(4) J. P. Heremans and V. Jovovic and E. S. Toberer and A. Saramat and K. Kurosaki and A. Charoenphakdee and S. Yamanaka and G. J. Snyder, Science, 321, 554 (2008).

(5) K. Biswas and J. He and I. D. Blum and C.-I. Wu and T. P. Hogan and D. N. Seidman and V. P. Dravid and M. G. Kanatzidis, Nature 489, 414 (2012).

(6) A.Saramat and G. Svensson and A. E. C. Palmqvist and C. Stiewe and E. Mueller and D. Platzek and S. G. K. Williams and D. M. Rowe and J. D. Bryan and G. D. Stucky, J. Appl. Phys. 99, 023707 (2006).

(7) S. R. Culp and J. W. Simonson and S. J. Poon and V. Ponnambalam and J. Edwards and T. M. Tritt, Appl. Phys. Lett. 93, 022105 (2008).

(8) B. C. Sales and D. Mandrus and R. K. Williams, Science, 272, 1325 (1996).

(9) D. J. Singh and I. I. Mazin, Phys. Rev. B 56, R1650 (1997).

(10) V. Keppens and D. Mandrus and B. C. Sales and B. C. Chakoumakos and P. Dai and R. Colda and M. P. Maple and D. A. Gajewski and E. J. Freeman and S. Bennington, Nature 395, 876 (1998).

(11) O. Bubnova and Z. U. Khan and H. Wang and S. Braun and D. R. Evans and M. Fabretto and P. Hojati-Talemi and D. Dagnelund and J.-B. Arlin and Y. H. Geerts and S. Desbief and D. W. Breiby and J. W. Andreasen and R. Lazzaroni and W. M. Chen and I. Zozoulenko and M. Fahlman and P. J. Murphy and M. Berggren and X. Crispin, Nature Mater. 13, 190 (2014).

Physical Chemistry Chemical Physics Accepted Manuscript

(12) D. Wang and W. Shi and J. Chen and Z. Shuai, Phys. Chem. Chem. Phys., 14, 16505 (2012).

(13) Q. Wei and M. Mukaida and Y. Naitoh and T. Ishida, Adv. Mater. 25, 2831 (2013).

(14) Q. Wei and M. Mukaida and K. Kirihara and Y. Naitoh and T. Ishida, RSC. Adv. 4, 28802 (2014).

(15) H. Nakamura and T. Ohto and T. Ishida and Y. Asai, J. Am. Chem. Soc. 135, 16545 (2013).

(16) J. P. Bergfield and C. A. Stafford, Nnao Lett. 9, 3072 (2009).

(17) C. Finch and V. Garcia-Suarez and C. Lambert, Phys. Rev. B 79, 033405 (2009).

(18) S.-H. Ke and W. Yang and S. Curtarolo and H. U. Baranger, 9, 1011 (2009).

(19) G-H. Kim and L. Shao and K. Zhang and K. P. Pipe, Nature Mater. 12, 719 (2013).

(20) H. Zhang and D. V. Talapin, Angew. Chem. Int. Ed. 53, 9126 (2014).

(21) H. Liu and X. Shi and F. Xu and L. Zhang and W. Zhang and L. Chen and Q. Li and C. Uher and T. Day and G. J. Snyder, Nature Mater. 11, 422 (2013).

(22) B. Yu and W. Liu and S. Chen and H. Wang and H. Wang and G. Chen and Z. Ren, Nano Energy 1, 472 (2012).

(23) L-D. Zhao and S.-H. Lo and Y. Zhang and H. Sun and G. Tan and C. Uher and C. Wolverton and V. P. Dravid and M. G. Kanatzidis, Nature 508, 373 (2014).

(24) C-L. Chen and H. Wang and Y-Y. Chen and T. Day and G. J. Snyder, J. Mater. Chem. A 2, 11171 (2014).

(25) S. Sassi and C. Candolfi and J.-B. Vaney and V. Ohorodniichuk and P. Masschelein and A. Dauscher and B. Lenoir, Appl. Phys. Lett. 104, 212105 (2014).

Physical Chemistry Chemical Physics Accepted Manuscript

(26) G. Dennler and R. Chmielowski and S. Jacob and F. Capet and P. Roussel and S. Zastrow and K. Nielsch and I. Opahle and G. K. H. Madsen, Adv. Energy Mater. 4, 1301581 (2014).

(27) T. Chattopadhyay and J. Pannetier and H. G. Vonschnering, J. Phys. Chem. Solids 47, 879 (1986).

(28) W. J. Baumgardner and J. J. Choi and Y.-F. Lim and T. Hanrath, J. Am. Chem. Soc. 132, 9519 (2010).

(29) T. J. Scheidemantel and C. Ambrosch-Draxl and T. Thonhauser and J. V. Badding and J. O. Sofo, Phys. Rev. B 68, 125210 (2003).

(30) G. K. H. Madsen and D. J. Singh, Comp. Phys. Comm. 175, 67 (2006).

(31) D. Parker and D. J. Singh, J. Appl. Phys. 108, 083712 (2010).

(32) C. Bera and S. Jacob and I. Opahle and N. S. H. Gunda and R. Chmielowski and G. Dennler and G. K. H. Madsen, Phys. Chem. Chem. Phys. 16, 19894 (2014).

(33) L. Xi and Y. B. Zhang and X. Y. Shi and J. Yang and X. Shi and L. D. Chen and W. Zhang and J. Yang and D. J. Singh, Phys. Rev. B 86, 155201 (2012).

(34) P. García-Fernández and M. Verissimo-Alves and D. I. Bilc and P. Ghosez and J. Junquera, Phys. Rev. B 86, 085305 (2012).

(35) J. J. Pulikkotil and D. J. Singh and S. Auluck and M. Saravanan and D. K. Misra and A. Dhar and R. C. Budhani, Phys. Rev. B 86, 155204 (2012).

(36) K. P. Ong and D. J. Singh and P. Wu, Phys. Rev. B 83, 115110 (2011).

(37) D. J. Singh, Phys. Rev. B 81, 195217 (2010).

(38) L. Zhang and M.-H. Du and D. J. Singh, Phys. Rev. B 81, 075117 (2010).

(39) M.-S. Lee and F. P. Poudeu and S. D. Mahanti, Phys. Rev. B 83, 085204 (2011).

Physical Chemistry Chemical Physics Accepted Manuscript

(40) G. K. H. Madsen, J. Am. Chem. Soc. 128, 12140 (2006).

(41) K. Tyagi and B. Gahtori and S. Bathula and S. Auluck and A. Dhar, Appl. Phys. Lett. 105, 173905 (2014).

(42) D. F. Zou and S. H. Xie and Y. Y. Liu and J. G. Lin and J. Y. Li, J. Appl. Phys. 113, 193705 (2013).

(43) C. Sevik and T. Cagin, Appl. Phys. Lett. 95, 112105 (2009).

(44) X. Chen and Y. Wang and Y. Ma and T. Cui and G. Zou, J. Phys. Chem. C, 113, 14001 (2009).

(45) D. Zou and S. Xie and Y. Liu and J. Lin and J. Li, J. Alloys Comp. 570, 150 (2013).

(46) J. Yang and G. Yang and G. Zhang and Y. X. Wang, J. Mater. Chem. A 2, 13923 (2014).

(47) H. Balout and P. Boulet and M.-C. Record, J. Phys. Chem. C 118, 19635 (2014).

(48) R. Guo, X. Wang, Y. Kuang, B. Huang, Phys. Rev. B 92, 115202 (2015)

(49) A. J. Hong, L. Li, H. X. Zhu, Z. B. Yan, J.-M. Liu, Z. F. Ren, J. Mater. Chem. A 3, 13365 (2015).

(50) K. Kutorasinski, B. Wiendlocha, S. Kaprzyk, J. Tobola, Phys. Rev. B 91, 205201 (2015).

(51) G. Shi and E. Kioupakis, J. Appl. Phys. 117, 065103 (2015).

(52) J. M. Soler and E. Artacho and J. D. Gale and A. García and J. Junquera and P. Ordejón and D. Sánchez-Portal, J. Phys.: Condens. Matter 14, 2575 (2002).

(53) J. P. Perdew and K. Burke and M. Ernzerhof, Phys. Rev. Lett. 77, 3865 (1996).

Physical Chemistry Chemical Physics Accepted Manuscript

(54) G. Pizzi and D. Volja and B. Kozinsky and M. Fornari and N. Marzari, Comp. Phys. Comm. 185, 422 (2014).

(55) B.-L. Huang and M. Kaviany, Phys. Rev. B 77, 125209 (2008).

(56) K. Durczewski and M. Ausloos, Phys. Rev. B 61, 5303 (2000).

(57) T. Okuda and K. Nakanishi and S. Miyasaka and Y. Tokura, Phys. Rev. B 63, 113104 (2001).

(58) E. Flage-Larsen and Ø. Prytz, Appl. Phys. Lett. 99, 202108 (2011).

(59) A. Filippetti and P. Delugas and M. J. Verstraete, I. Pallecchi and A. Gadaleta and D. Marré and D. F. Li and S. Gariglio and V. Fiorentini, Phys. Rev. B 86, 195301 (2012).

(60) P. Delugas and A. Filippetti and M. J. Verstraete and I. Pallecchi and D. Marré and V. Fiorentini, Phys. Rev. B 88, 045310 (2013).

(61) M. J. Peters and L. E. McNeil, Phys. Rev. B 41, 5893 (1990).

(62) H. Wiedemeier and H. G. von Schnering, Z. Kristallogr, 148, 295 (1978).

(63) Q. Tan and L.-D. Zhao and J.-F. Li and C.-F. Wu and T.-R. Wei and Z.-B. Xing and M. G. Kanatzidis, J. Mater. Chem. A 2, 17302 (2014).

(64) T. Tadano and Y. Gohda and S. Tsuneyuki, J. Phys.: Condens. Matter 26, 225402 (2014).

(65) T. Tadano and Y. Gohda and S. Tsuneyuki, Phys. Rev. Lett. 114, 095501 (2015).

Physical Chemistry Chemical Physics Accepted Manuscript

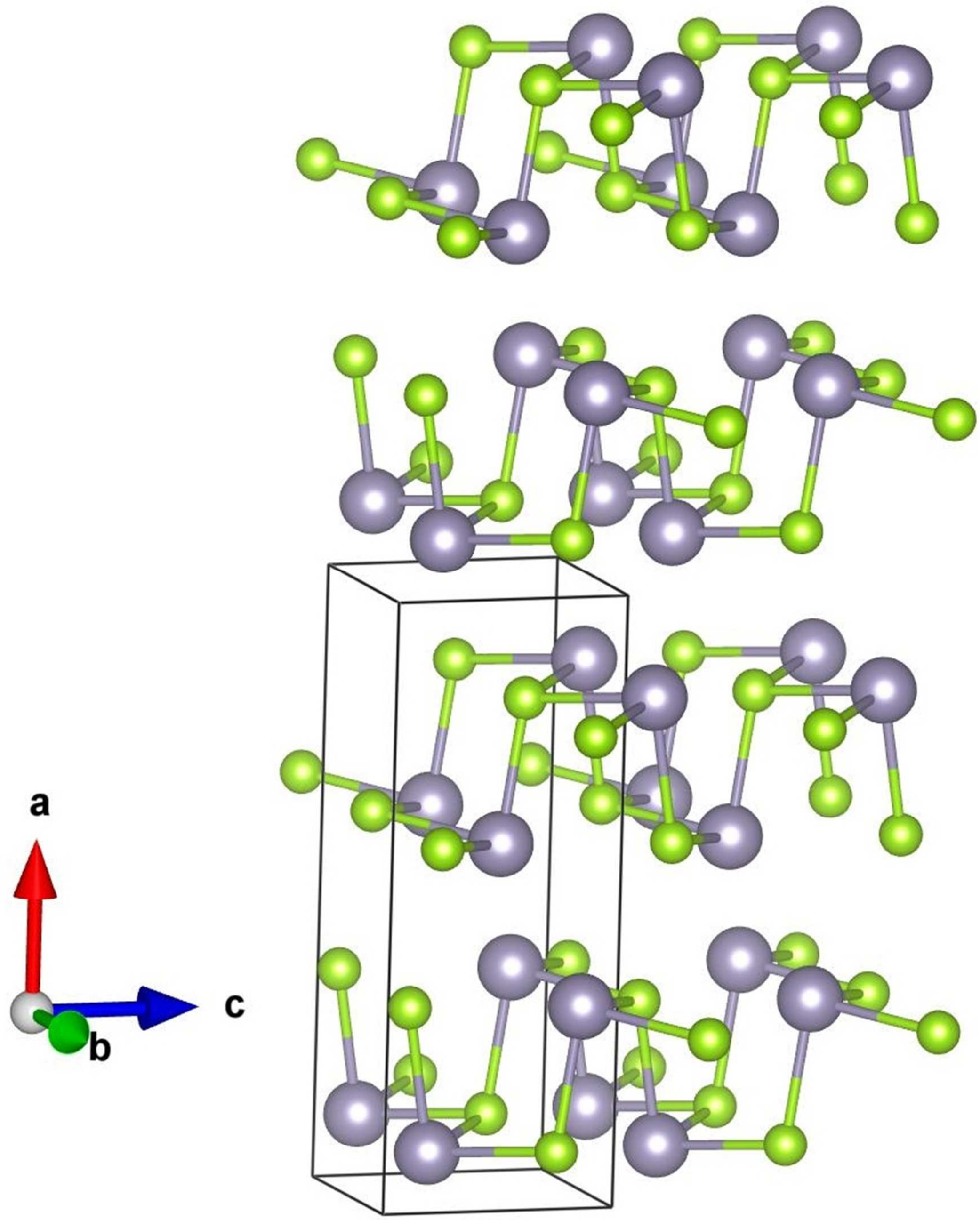

Figure1. Crystal structure of the low-temperature *Pnma* phase of SnSe. The primitive cell is shown as black line lattice. Gray larger balls are Sn atoms and green smaller balls are Se atoms. The directions of three axes (a, b, and c) are also shown as red, green and blue arrows, respectively. (Color online)

Physical Chemistry Chemical Physics Accepted Manuscript

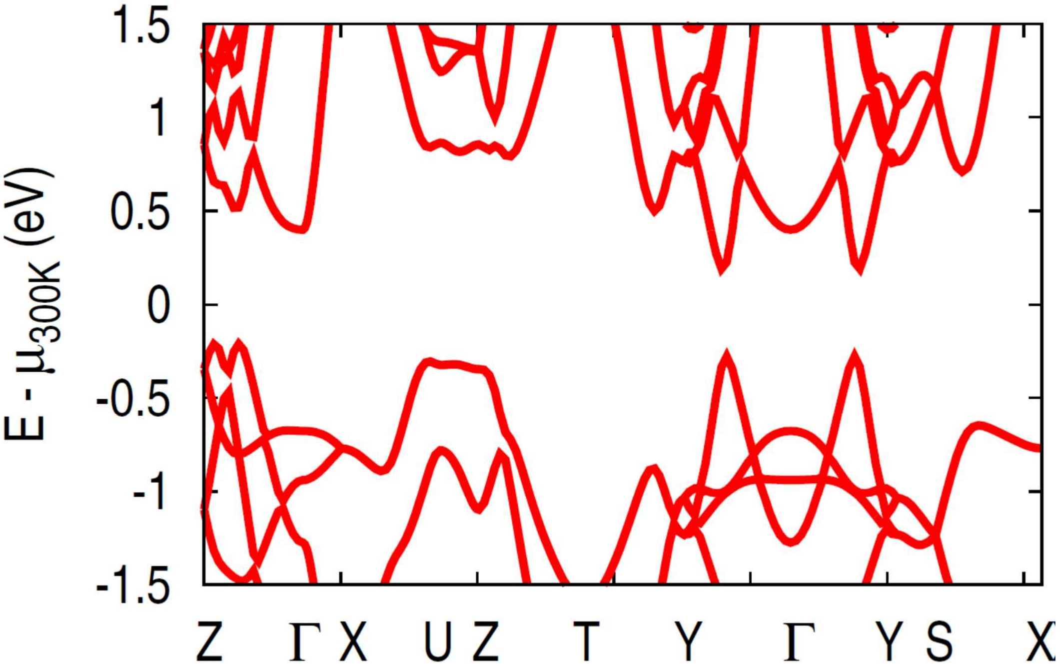

Figure2. The calculated band structure of the low-temperature *Pnma* phase of SnSe.

Physical Chemistry Chemical Physics Accepted Manuscript

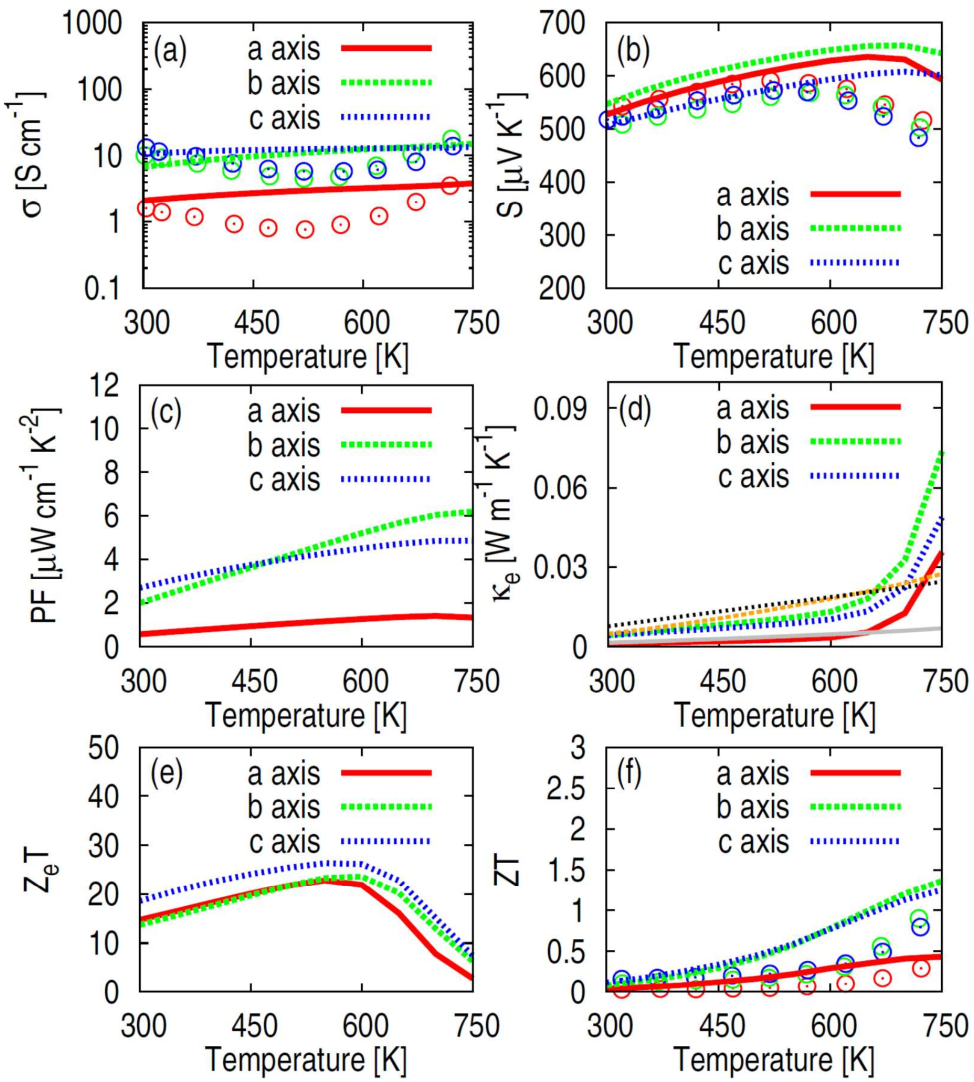

Figure3. The calculated thermoelectric properties as a function of temperature for the *Pnma* phase of the undoped SnSe crystal. (a) Electrical conductivity σ. (b) Seebeck coefficient S. (c) Power factor (PF) $S^2\sigma$. (d) Electronic contribution to thermal conductivity κ_e. The values predicted by Wiedemann-Franz (WF) law $L\sigma T$ are also plotted (a axis: gray solid, b axis: orange dashed, c axis: black dotted). (e)$Z_eT = \frac{S^2\sigma}{\kappa_e}T$. (f) $ZT = \frac{S^2\sigma}{\kappa_e+\kappa_l}T$. All quantities are plotted along all three axial directions (a axis: red solid, b axis: green dashed, c axis: blue dotted). In (a), (b) and (f), experimental values reported in Ref. 23 are also plotted with open circles (a axis: red circle, b axis: green circle, c axis: blue circle).

Physical Chemistry Chemical Physics Accepted Manuscript

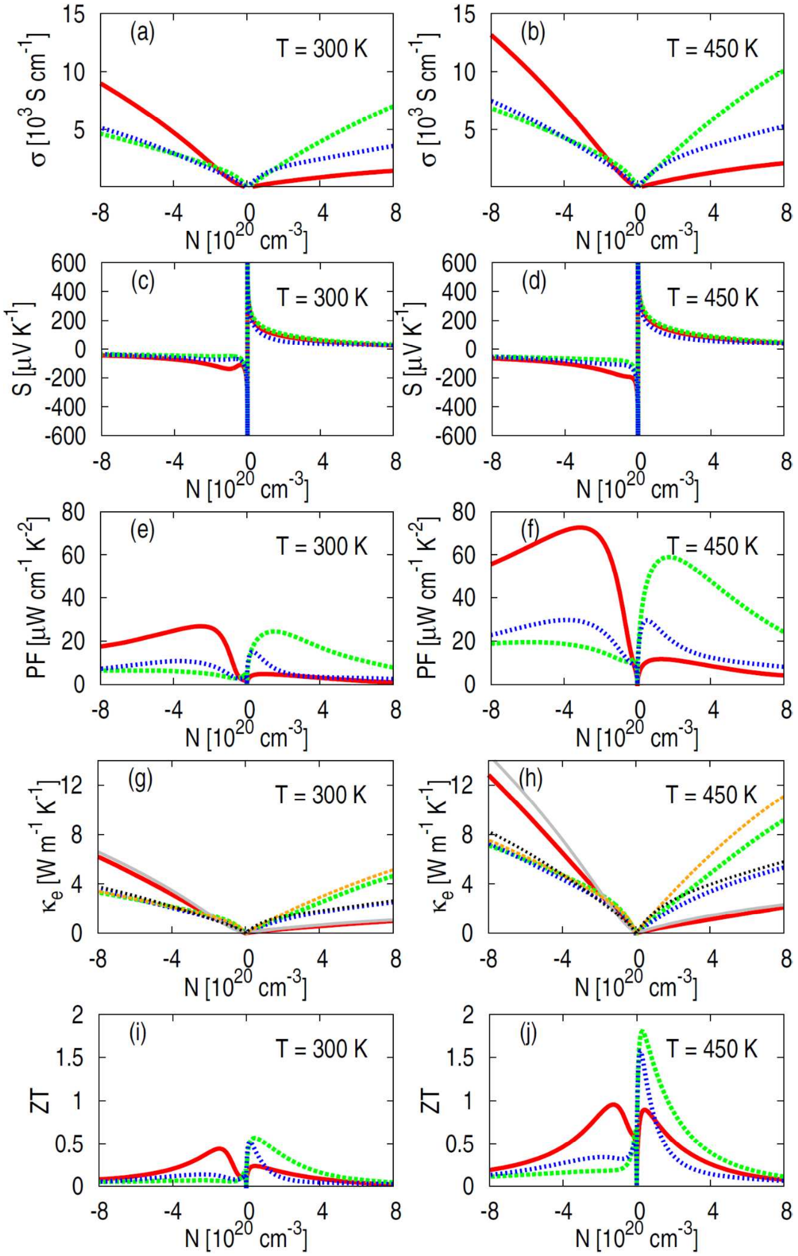

Figure4. The calculated *σ*, *S*, PF, κ_e, and *ZT* as a function of carrier concentration at 300K ((a), (c), (e), (g), (i), respectively) and 450K ((b), (d), (f), (h), (j), respectively). The positive carrier concentration corresponds to the holes (p-type doping), and the negative corresponds to the electrons (n-type doping). The values along all three directions (a axis: red solid, b axis: green dashed, c axis: blue dotted) are plotted. In (g) and (h), $\kappa_e^{WF} = L\sigma T$ are also plotted (a axis: gray solid, b axis: orange dashed, c axis: black dotted).

Physical Chemistry Chemical Physics Accepted Manuscript

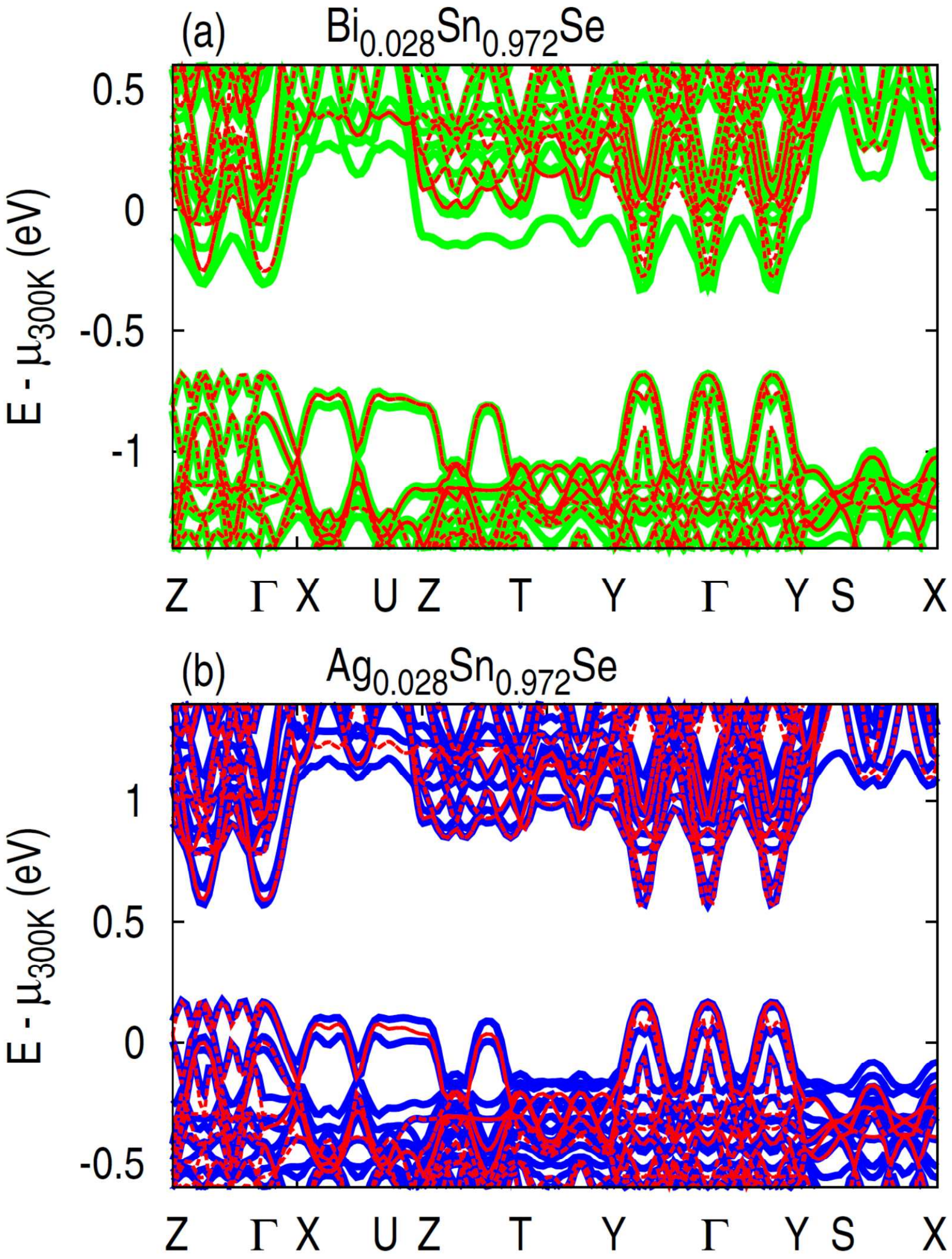

Figure5. The calculated band structure of $Bi_{0.028}Sn_{0.972}Se$ ((a), green solid line) and $Ag_{0.028}Sn_{0.972}Se$ ((b), blue solid line). The band of the undoped SnSe (1×3×3) supercell (red dashed line) is also shown in both panels. All bands are plotted along the same symmetry line used for plotting the band of the primitive cell (Fig. 2).

Physical Chemistry Chemical Physics Accepted Manuscript

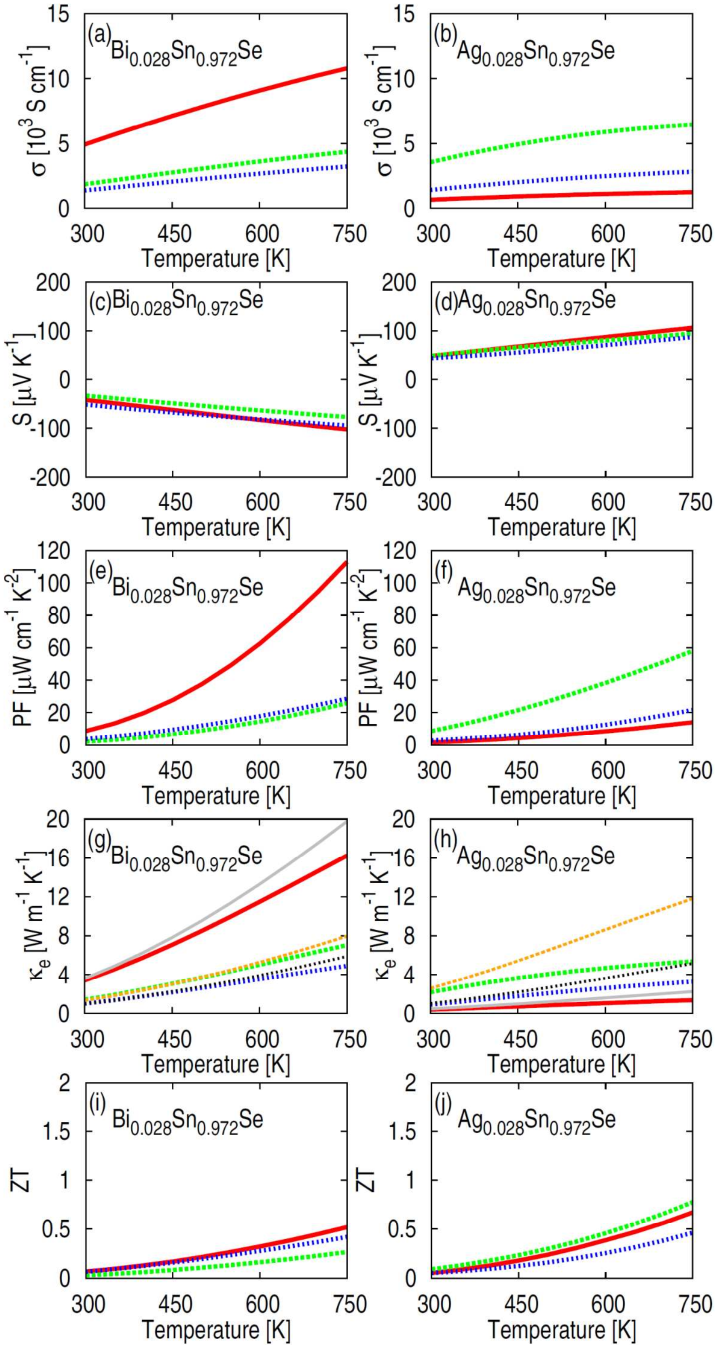

Figure6. The calculated σ, S, PF, κ_e, and ZT as a function of temperature for $Bi_{0.028}Sn_{0.972}Se$ ((a), (c), (e), (g), (i), respectively) and $Ag_{0.028}Sn_{0.972}Se$ ((b), (d), (f), (h), (j), respectively). Values along all three axial directions are plotted (a axis: red solid, b axis: green dashed, c axis: blue dotted). In (g) and (h) $\kappa_e^{WF} = L\sigma T$ are also plotted (a axis: gray solid, b axis: orange dashed, c axis: black dotted).

Physical Chemistry Chemical Physics Accepted Manuscript

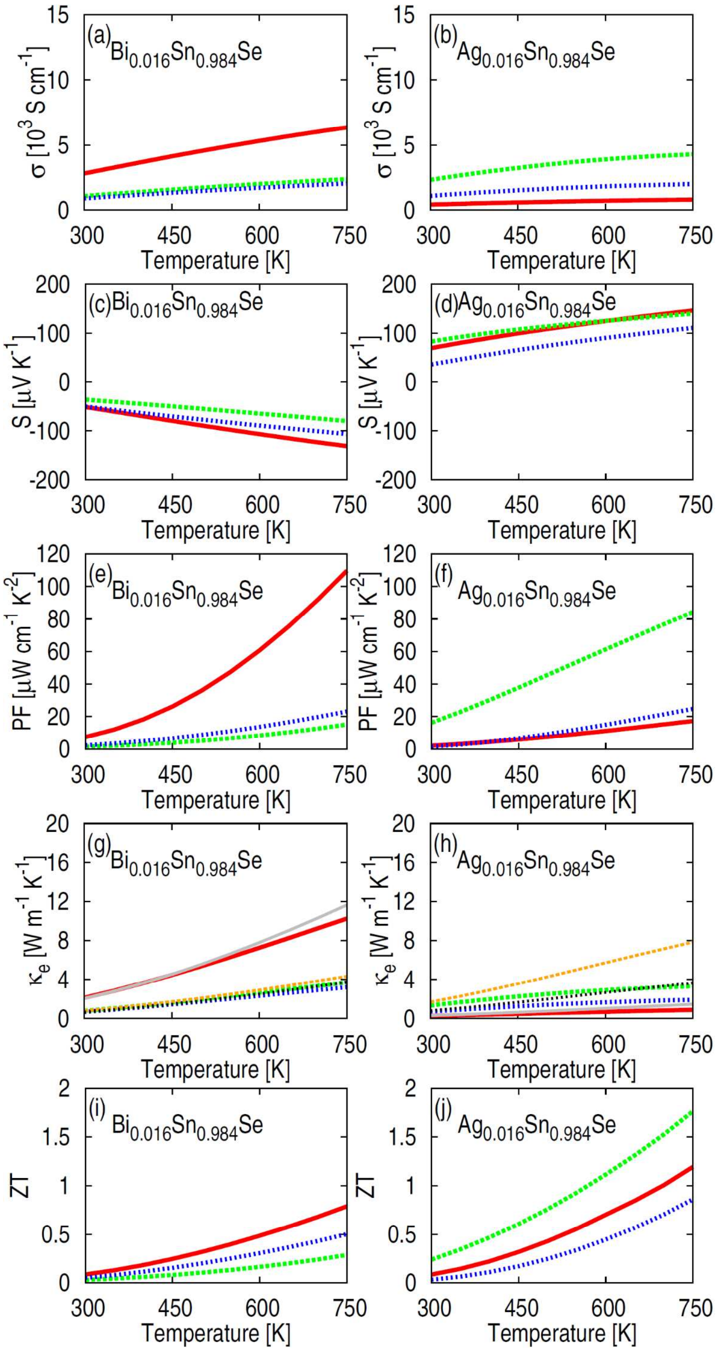

Figure7. The calculated *σ*, *S*, PF, κ_e, and *ZT* as a function of temperature for $Bi_{0.016}Sn_{0.984}Se$ ((a), (c), (e), (g), (i), respectively) and $Ag_{0.016}Sn_{0.984}Se$ ((b), (d), (f), (h), (j), respectively). Values along all three axial directions are plotted (a axis: red solid, b axis: green dashed, c axis: blue dotted). In (g) and (h) $\kappa_e^{\mathrm{WF}} = L\sigma T$ are also plotted (a axis: gray solid, b axis: orange dashed, c axis: black dotted).

Physical Chemistry Chemical Physics Accepted Manuscript